EPS-HEP 95 Ref. eps0533
Submitted to Pa 9
Pl 12

DELPHI 95-73 PHYS 508
30 June, 1995

Update to the search for the Z^0 decay into a Higgs boson and a Photon

DELPHI Collaboration

Paper submitted to the "EPS-HEP 95" Conference
Brussels, 27th July-2nd August 1995

EPS-HEP 95 Ref. eps0533
Submitted to Pa 9
Pl 12

DELPHI 95-73 PHYS 508
30 June, 1995

Update to the search for the Z^0 decay into a Higgs boson and a Photon

Preliminary

DELPHI Collaboration

J.A. Barrio[1] , J.L. Contreras[1] , A. López-Fernández[2]

Abstract

A search for the associated production of a Higgs boson and a photon has been carried out in the data sample collected by DELPHI through the years 1991 to 1994, corresponding to approximately 3.2 million hadronic Z^0 decays. Preliminary results are presented.

The analysis is based on the detection of events containing an isolated photon plus two jets. The complementarity between the $b\overline{b}$ and the $\tau^+\tau^-$ decay modes of the Higgs boson is used to cover a wide range of Higgs boson masses. In both modes the kinematical reconstruction of the event provides a good mass resolution with little dependance on the photon energy.

The increase in statistics and the technical improvements of the analysis contribute to set a more stringent limit on the branching ratio $Z^0 \to H\gamma$ compared to the 1994 analysis. For the Higgs mass domain covered by the present search, the limits obtained so far put severe constraints on anomalous triple boson couplings which are not excluded by the results of LEP/SLC and the Tevatron.

[1]Universidad Complutense de Madrid
[2]Universidad Autonoma de Madrid

1 Introduction

The reaction $Z^0 \to H\gamma$ or $Z^0 \to S\gamma$ has been used previously [1] [2], to look for the existence of Higgs bosons (H) and more general kinds of scalars (S) predicted by a variety of models. This paper describes the results of a search for $Z^0 \to H\gamma$. The Higgs boson decay modes searched for are: $q\overline{q}$, $b\overline{b}$ and $\tau^+\tau^-$. The sample analyzed comprises the whole data collected by DELPHI detector from 1991 to 1994, for $q\overline{q}$ and $b\overline{b}$; and from 1992 to 1993, for the $\tau^+\tau^-$ sample. With respect to previous analyses it benefits from increased statistics, the inclusion of the search for $H \to \tau^+\tau^-$ to cover the low mass region and various technical improvements. It supersedes the results published in references [1].

The paper begins with a brief theoretical introduction of the expected theoretical production mechanisms, H decay modes and the experimental backgrounds and search strategies. Section 3 describes the identification criteria for Z^0 decays with isolated photons, including the $q\overline{q}\gamma$ and $\tau^+\tau^-\gamma$ selections. Section 4 deals with the mass reconstruction. Section 5 is devoted to background estimations. The results are finally reported in section 6 where a limit on the $Z^0 \to H\gamma$ is extracted and compared to non-standard expectations.

2 $H\gamma$ production and detection

2.1 Higgs boson production

In the Standard Model framework the decay of the Z^0 boson into the Higgs boson can mainly take place via the reactions:

$$Z^0 \to HZ^* \tag{1}$$

and

$$Z^0 \to H\gamma, \tag{2}$$

Compared to process (1), the matrix element of reaction (2) is subject to a strong suppression due to the vanishing direct coupling between the Z^0 , the neutral Higgs boson and the photon. Reaction (2) can thus take place only in higher orders, through loops of $W^\pm$ bosons and massive charged fermions, with the amplitude being largely dominated by the $W^\pm$ loop.

In the Standard Model the partial width for the $Z^0 \to H\gamma$ decay can be written in the form:

$$\Gamma^{SM}(Z^0 \to H\gamma) = \frac{E_\gamma^3}{12\pi}\left(\frac{eg^2}{16\pi^2 m_W}\right)^2 A_{SM}^2 \tag{3}$$

where $E_\gamma = (m_Z^2 - m_H^2)/(2m_Z)$ is the energy of the photon recoiling against the Higgs particle, g is the SU(2) coupling constant and

$$A_{SM} \simeq -\left(4.55 + 0.31\left(\frac{m_H}{m_W}\right)^2\right). \tag{4}$$

For a derivation of this expression see for example reference [3]. Despite the matrix element suppression, for relatively large H masses the two-body phase space factor favors the $Z^0 \to H\gamma$ decay with respect to reaction (1), so that, for example,

$$\frac{BR(Z^0 \to H\gamma)}{BR(Z^0 \to H\mu^+\mu^-)} > 1 \tag{5}$$

when $m_H > 60\ GeV$.

However the potentiality of the $Z^0 \to H\gamma$ decay in the search for the Standard Model Higgs boson at LEP remains small. This is due to the presence of the large background of $Z^0 \to f\overline{f}$ events where the $Z^0 \to H\gamma$ topology is faked by isolated photons from Final State Radiation (FSR) and/or unresolved pairs of photons from decays of neutral pions. As a consequence the present limits on the $Z^0 \to H\gamma$ decay are about one order of magnitude larger than the Standard Model predictions [1],[2], while the limit on the H mass comes from the search of the almost background free Bjorken process (1) with the virtual Z^0 decaying into neutrinos or charged leptons.

This scenario can change outside the Standard Model. In the MSSM the $W^{\pm}$ loop term can be decreased, while a contribution from chargino loops may increase the rate for this processes by up to a factor of 3 with respect to the SM value [5]. The minimal supersymmetric prediction, as the SM prediction, is thus below the level of sensitivity provided by present LEP experiments.

Another approach to the problem lies in the use of effective Lagrangians which parameterize the possible anomalous couplings of the H to the vector bosons. In [7], the $ZH\gamma$ vertex is described by means of an effective dimension-six term in the interaction lagrangian density:

$$L_{effec} = \sum_{i}^{7} \frac{f_i}{\Lambda^2} Oi \tag{6}$$

Where O_i are the operators which represent the anomalous couplings considered, the unknown dimensioned constant Λ in the denominator, the typical energy scale of the new interactions responsible of them, and f_i the constants which define the strength of each term.

Strict bounds for some of the coefficients $\frac{f_i}{\Lambda^2}$ are obtained from low energy data, while for others the restrictions are loose. These still leave the possibility of a large enhancement for the $Z^0 \to H\gamma$ decay width, although the request of *natural* values for the weakly bound coefficients (that they should be of the same order as the strongly bounded ones) would effectively constrain the amplification with respect to the Standard Model.

The same kind of arguments apply to the decay $H \to \gamma\gamma$, whose branching ratio could also be sizeable. If both processes are enhanced the result would be seen as $\gamma\gamma\gamma$ final states. The search for the process $Z^0 \to \gamma\gamma\gamma$ is therefore complementary to the present one and both contribute to set limits to the possible anomalous Higgs couplings.

2.2 Decay modes

In the range of masses of interest for this study the Higgs boson should almost exclusively decay into couples of opposite-sign fermions. The branching ratio of each kind of fermion is proportional to the the square of its mass. Thus, far away from the threshold regions, where production of a new kind of particles opens, the H branching ratio is dominated by the particle of highest mass among those whose production is possible. In order to cover a wide range of possible H masses, three different decay channels have been considered in the present analysis: $\tau^+\tau^-$, $q\overline{q}$ and $b\overline{b}$. The channel $q\overline{q}$ refers to the case where the H decays to a hadronic state of unspecified flavor. Final states should include therefore a couple of opposite-sign tau leptons, or of hadronic jets, recoiling against an isolated photon. In the later case a further selection will require b quark identification (*b-tag*) of the hadronic system.

The region of masses studied goes from 5 to 70 GeV. The lower limit is imposed by technical limitations in the method used. The upper range is limited by the growing contamination from events where a neutral pion fakes an isolated γ and real FSR photons. From 5 GeV to around 9 GeV $\tau^+\tau^-$ and $c\overline{c}$ production dominate, while for H masses greater than around 11 GeV $b\overline{b}$ branching ratio exceeds 80% [19]. In between, there is a thin transition region where the exact behavior depends on the running b quark mass with some theoretical uncertainties. The three regions just described will be named as region I (5-9 GeV), II (9-11 GeV) and III (11-70 GeV) respectively and will be considered differently in the final analysis.

3 The selection of Z^0 events with isolated photons

A detailed description of the DELPHI detector can be found in reference [4]. Its main features used in the present analysis are the precise measurement of tracks in the microvertex detector (VD) [9] and the detection of electromagnetic energy clusters in the barrel electromagnetic calorimeter, the High density projection chamber (HPC), and the forward electromagnetic calorimeter (FEMC).

3.1 $q\overline{q}\gamma$ sample

3.1.1 Hadronic selection

Events with isolated photons were extracted from the multihadronic sample collected by DELPHI in the years 1991 to 1994, corresponding to approximately 3.2 millions of hadronic Z^0 decays. The hadronic event selection is based on the request of large charged multiplicity ($N_{ch} \geq 5$) and high visible energy ($E_{vis} \geq 12\%\sqrt{s}$). These cuts select a sample of 3,062,370 reconstructed hadronic Z^0 decays, including less than 1% from leptonic final states. Their total efficiency is $95.4 \pm 0.2\%$ for hadronic Z^0 decays.

3.1.2 Photon identification

The candidates for the $Z^0 \to H\gamma$ decay, where the H decays into a $q\overline{q}$ pair, were selected by requiring the presence of at least an energetic *neutral* shower in the DELPHI electromagnetic calorimeters[3] satisfying the standard DELPHI photon identification criteria [12]. Among these, we can mention:

- the shower shape should be compatible with that expected for single electromagnetic deposit.
- showers consistent with being originated by bremsstrahlung off an electron in the DELPHI material are rejected.
- photons converting into an electron-positron pair when crossing the detectors passive material before arriving to the electromagnetic calorimeters are also reconstructed.

After these quality criteria, additional cuts were applied in order to reduce the background contamination of Initial State Radiation photons and of energetic neutral pions.

[3]See reference [4] for a detailed description of the DELPHI detector.

- a minimum energy (E_γ) of 5.5 GeV should be assigned to the photon,
- the polar angle of this photon with respect to the beam axis should be outside the region defined by $|\cos\theta_\gamma| < 0.95$,
- no charged particles with energy $E > 500$ MeV should be reconstructed in a cone of 20^o centered around the photon direction.
- the total neutral energy in the same 20^o cone should be lower than 1 GeV.

As a large contamination of photons from FSR still survives after the above criteria, a more severe isolation condition was added to the previous cuts. This condition will depend on the hadronic mass recoiling against the photon candidate and is described in section §4.3.

3.1.3 b-tagging

As noted in the introduction, for a wide range of H masses the production of $b\overline{b}$ is its dominant decay mode. For what concerns the background , FSR off b quarks is disfavored due to the electric charge and isolated high energy neutral pions should mostly come from the fragmentation of light quarks. These two reasons point to the idea of using a b-tagging procedure to increase the signal over background ratio in this region.

The good resolution of the DELPHI microvertex detector allows an efficient vertex tagging of b decays. The procedure used is described in [8]. Its final output is a variable which can be interpreted as the probability that all the tracks of the event come from the common primary vertex.

During the first data taking period covered by this analysis, the 1991,1992 and 1993 runs, the DELPHI vertex detector consisted in three layers of single sided silicon microstrip detectors. Its full polar coverage extended from 43^o to 137^o, giving most of the times 3 points per track in the plane normal to the beam. For the 1994 run, double sided detectors were included in the closer and outer layers, and the angular acceptance was increased; details of this upgrade can be found in reference [20]. Nevertheless, as the understanding of the double sided information is still progressing, for the present study only information in the plane normal to the beam was used.

In both periods the use of the average interaction point improved the determination of the event vertex and thus the b-tagging probability variable.

For the chosen value of the cut in the tagging variable, the use of this technique on simulated signal events shows that its efficiency before isolation cuts depends on the mass of the H. Table 1 shows the efficiency for the signal as a function of the H mass after isolation cuts, before and after b-tagging have been applied.

3.2 $\tau\tau\gamma$ sample

3.2.1 Leptonic selection

The data analyzed comprise the full statistics recorded by DELPHI during 1992 and 1993, corresponding to approximately 1,500,000 hadronic decays of the Z^0 .

The first step of the selection was designed to extract leptonic decays of the Z^0 . Thus, events should have between two and four charged tracks coming from the interaction

region, within 1.5 cm in the plane transverse to the beam and 4.5 cm in the direction parallel to the beam, and having a polar angle between 25° and 155° . These tracks had to be clustered into two jets using the LUCLUS algorithm [11] (with d_{join} = 2 GeV) and both jets should have a total momentum higher than 0.5 GeV/c. Events with a 2-2 topology were rejected. In order to suppress two-photon interactions the total energy measured in the event had to be above $25\%\sqrt{s}$. Finally, a cut was applied to reduce the background due to hadronic events where some tracks are lost at low polar angles. It was required that, for events with three or four tracks, the polar angle of the most energetic jet should lie between 32° and 148°.

3.2.2 Photon identification

The candidates for the $Z^0 \rightarrow H\gamma$ decay, where the H decays to a $\tau^+\tau^-$ pair, were selected by requiring the presence of at least an energetic *neutral* shower in the DELPHI electromagnetic calorimeters. Again, standard DELPHI photon identification criteria [12] were applied (See §3.1.2).

Further cuts were applied in order to obtain a sample of $l^+l^-\gamma$ events with an isolated photon:

- the most energetic photon should have more than 10 GeV,
- the polar angle of this photon with respect to the beam axis should lie in the region $20^o < \theta_\gamma < 160^o$,
- the photon should have an isolation angle above 13° with respect to the direction of the nearest jet. Further isolated photons were allowed if they had an energy lower than 3 GeV,
- the sum of the angles between the two jets and the isolated photon was required to be above 340°.

The isolation requirement was made in order to eliminate low energy FSR photons or photons coming from π^0s in the decays of the taus, which are always close to the charged decay products. The cut in polar angle reduces the ISR contribution. Finally, the cut in the sum of angles was applied to reduce the contaminations from two-photon interactions.

3.2.3 τ selection

As the next step, $\tau\tau\gamma$ events were separated from $ee\gamma$ and $\mu\mu\gamma$. Defining $P_{mx,i}$ as the momentum of the most energetic charged particle in the *ith* jet, it was required that $(P_{mx,1} + P_{mx,2}) < K_1 \times \sqrt{s}$, where $\sqrt{s}$ was the centre-of-mass energy. The value of the cut K_1 changes from the barrel region ($K_1 = 0.45$) to the forward ($K_1 = 0.35$), where the reconstruction of the momentum is poorer, specially for electrons.

Similarly, defining $E_{em,i}$ as the sum of the energies of all the electromagnetic clusters within 10° of the direction of the *ith* jet, it was requested that $\sqrt{E^2_{em,1} + E^2_{em,2}} < K_2 \times \sqrt{s}$. Again, K_2 varies from 0.35 to 0.25, depending on the quality of the energy reconstruction in each particular region. This cut is effective to reject $ee\gamma$ events.

An additional cut to reduce $ee\gamma$ and $\mu\mu\gamma$ background was applied requiring the transverse missing momentum to be above a minimum value, dependent on the H mass.

Further cuts were applied for H masses below 6 GeV to ensure good mass reconstruction by avoiding situations were some tracks of the event could be lost, namely, the photon should not point to a TPC crack, the event should not lie in the forward region, and should have their charges balanced.

Finally, it was required the H mass to be above 1.5 GeV, in order to reject very low mass events, with very little impact on the studied mass range.

4 Kinematical reconstruction

4.1 Method and mass resolution

The experimental resolution in determining the mass of the system recoiling against the photon candidate largely determines the detector sensitivity in the search for the $Z^0 \to H\gamma$ decay, as the expected signature is represented by a peak in this mass distribution. The recoiling mass, m_H, is usually determined from the photon energy E_γ and the center-of-mass energy $\sqrt{s}$ by means of the formula:

$$m_H^2 = s - 2\sqrt{s}E_\gamma. \tag{7}$$

The recoil mass resolution is therefore proportional to the photon energy resolution through the factor $\left(\frac{\sqrt{s}}{m_H}\right)$:

$$\delta m_H = \left(\frac{\sqrt{s}}{m_H}\right) \delta E_\gamma, \tag{8}$$

which implies a fast deterioration of the resolution as the mass decreases.

In order to achieve a better resolution the calorimetric information was thus complemented with the information from the reconstructed jets.

For the $q\overline{q}\gamma$ sample, these were built by applying the JADE [6] algorithm to all the reconstructed particles (excluding the photon itself) until precisely two jets were found. The procedure to construct tau jets was described in section §3.2.1 In both cases the measured jet masses and directions together with the photon direction and the beam energy constrain were used to get a measurement of the momentum of the two jets. In doing so, the mass of each jet, in the $q\overline{q}\gamma$ sample, was supposed to scale in the same proportion as its momentum. For the $\tau^+\tau^-\gamma$ sample, $m_{jet} = 0$ was assumed instead, approximation allowed by its high boost. The invariant mass of the fermionic system was obtained from the quantities derived above.

Combining this independent measure with the recoil mass computed from the photon energy measurement improved the mass resolution over the whole mass range. The gain is specially important at lower masses,where a factor 4 is achieved.

4.2 Quality cuts

The loss of particles due to inefficiencies or weak detector zones generates fake isolated photons. The above procedure allows us to identify these events, since the photon gets an artificially high reconstructed energy. A compatibility between the measured photon energy and the reconstructed one was therefore demanded. This cut is specially effective in the hadronic case.

4.3 Strict isolation

Even if the request of 20^0 isolation for the photon is enough to eliminate a big part of the background, it is clear that the optimum isolation cut depends on the mass of the H mass. The effect arises simply from the kinematic of the H decay process.

A variable isolation cut, with respect to the jet axis, was applied for each event once the estimated mass was known. For the $b\overline{b}\gamma$ sample, this cut was chosen so as to always keep the relative efficiency for the signal higher that 90%. Its values range from 120^0 for Higgs bosons masses of 20 GeV to 30^0 at 70 GeV. The extra rejection on the background varies from over 60% at low masses to 20% at 70 GeV. A similar cut was applied for the $\tau^+\tau^-\gamma$ sample, with an efficiency also around 90%.

This procedure is equivalent to a cut in the decay angle in the reference frame of the two jet system.

After this cut, final results on mass resolution and efficiency are shown in table **1** and **2**. Figure **1** shows the comparison between data and simulated hadronic events for the distribution of the reconstructed mass, and the relative proportions of neutral hadrons and photons according to the simulation. The agreement between the data and the simulation is satisfactory at low masses while discrepancies appear at high masses. This last fact corresponds to an already known effect, see for example reference [13].

Figure **2** represents the same comparison after b-tagging. The discrepancy between data and simulation is less marked in this case. Although not shown in the plot, according to the simulation the proportion of neutral hadrons is also considerably decreased, at high masses it is reduced but more than a factor of two with respect to the previous case.

Mass spectra for the $\tau^+\tau^-\gamma$ sample are shown in figure **3**

H mass (GeV)	Mass resolution	Efficiency before tagging	Efficiency after tagging
12.	1.5 ± 0.15 GeV	56 ± 1.5 %	30.0 ± 2 %
20.	1.9 ± 0.20 GeV	55.5 ± 1.5 %	27.0 ± 2 %
30.	2.1 ± 0.20 GeV	55 ± 1.5 %	25.0 ± 2 %
40.	2.4 ± 0.25 GeV	54 ± 1.5 %	23.0 ± 2 %
50.	2.2 ± 0.20 GeV	53 ± 1.5 %	23.0 ± 2 %
60.	2.6 ± 0.25 GeV	51 ± 1.5 %	24.5 ± 2 %
70.	2.0 ± 0.20 GeV	49.5 ± 1.5 %	26.0 ± 2 %

Table 1: Mass resolution and efficiency on simulated events before and after the b-tagging procedure. The values are normalized to the respective branching ratios. The errors reflect the the statistic of simulated events

5 Background estimation

As explained in the introduction, radiative events constitute an irreducible background to the signal. This is true in both the $q\overline{q}\gamma$ and $\tau^+\tau^-\gamma$ samples. It is therefore necessary to perform a background subtraction.

H mass (GeV)	Mass resolution	Efficiency
5.	2.0 ± 0.1	28.4 ± 0.6 %
7.	2.2 ± 0.1	31.9 ± 0.6 %
10.	2.3 ± 0.1	35.4 ± 0.6 %
15.	2.5 ± 0.1	36.3 ± 0.7 %
20.	2.6 ± 0.1	34.5 ± 0.6 %
30.	2.4 ± 0.1	33.7 ± 0.7 %
40.	2.4 ± 0.1	32.9 ± 0.7 %
50.	2.4 ± 0.1	33.7 ± 0.7 %
60.	2.3 ± 0.1	34.5 ± 0.7 %
70.	2.0 ± 0.1	34.1 ± 0.7 %

Table 2: Resolution and efficiency on simulated $H\gamma \to \tau^+\tau^-\gamma$ events. In both cases, errors comes from the Monte Carlo statistics

Two different methods were used to estimate the background contribution in the two samples considered. In the hadronic sample before b-tagging the number of candidates is sufficient to estimate precisely the shape of the background from the data itself. For the $\tau^+\tau^-\gamma$ and $b\overline{b}\gamma$ analysis, the Monte Carlo simulation was used.

For the $q\overline{q}\gamma$ sample, the analysis of the mass spectrum of the events which survive the isolation cuts was done at two levels: before and after applying the b-tagging procedure. At both steps a limit for the presence of an $H\gamma$ signal was obtained as a function of the reconstructed mass of the candidates.

Before b-tagging, with high statistics available and a smooth mass spectrum (see figure **1**), it is possible to estimate precisely the shape of the background. A smooth curve is obtained from the data.

After b-tagging the number of remaining events was too low to apply the above mentioned technique. In this case, the background was computed fitting a smooth curve to the simulated sample. Figure **2** shows a fair agreement between the tagged data and the corresponding curve. An statistical fluctuation is seen around 23 GeV with a probability around 3%, the candidate events in that mass region have been scanned and do not show any special characteristic. From this figure, it can also be concluded that the number of candidates below 60 GeV is very low and allows to set strict limits on the BR($Z^0 \to H\gamma$).

For the $H\gamma \to \tau^+\tau^-\gamma$ analysis, the background was estimated from Monte Carlo simulation. The KORALZ [14] generator was used for the $\tau^+\tau^-\gamma$ contamination. It takes into account both radiative events and neutral pions from τ decays. BABAMC [15] and DYMU3 [16] were used for the $e^+e^-\gamma$ and $\mu^+\mu^-\gamma$ contaminations, respectively. All generated events were processed through the detailed simulation of the DELPHI detector [17], to account for inefficiencies and reconstruction effects. As can be seen in figure **3**, a good agreement between this expected background and the $H\gamma \to \tau^+\tau^-\gamma$ candidates is found.

6 Results

No structure is evident from the mass distributions shown in figures **1,2** or **3**. Therefore, a limit on the possible contribution of a H signal was set. The method, common to the three analysis, proceeds as follows. For a given value of the H mass, a surrounding window is defined. The size of this window varies with mass and is chosen to keep 90 % of the signal, to take into account the small non-gaussian tails. Then, the number of background and candidate events inside this window is compared. From the difference, using the standard statistical techniques, the wanted limit is computed.

Figure **4** shows the limits on BR ($Z^0 \to H\gamma$) $\times$ BR ($H \to f\overline{f}$) for the three analysis. In the hadronic case a clear gain, a factor of two to three, is due to the use of b-tagging

The above limits are very general and therefore apply to a wide range of models. The next step is to translate them into a Standard Model limit. For this purpose, the mass spectrum was divided in the three regions defined in §2.2. Inside each of them, the SM limit was computed using the calculations of reference [19] as follows:

- Region I (5 - 9 GeV) The limit is based on the $\tau^+\tau^-\gamma$ analysis. Its branching ratio varies from $\sim$ 30% at 5 GeV to $\sim$ 60% at 9 GeV.
- Region II (9 - 11 GeV) To avoid the threshold uncertainties the worst limit among the 3 analysis presented was chosen. It turns out to be the one coming from the $q\overline{q}\gamma$ analysis.
- Region III (11 - 70 GeV) The limit is based on the $b\overline{b}\gamma$ analysis, which is dominant.

The resulting limits range from 5×10^{-6} in the best case to 3×10^{-5} in the worst case. The result are shown in figure **5**.

Although still a factor of 5 away from the Standard Model expectations, these limits become already relevant for some regions of the SUSY parameter space; and restrict a considerable region of the parameter space for allowed anomalous couplings of the H.

It should be noted that anomalous Higgs boson couplings may also enhance the branching ratio BR($H \to \gamma\gamma$) by several orders of magnitude [7]. In this case the resulting final state is 3γ and the previously published limits on BR($Z \to \gamma\gamma\gamma$) apply. In reference [10] the limit obtained is BR($Z \to \gamma\gamma\gamma$) $\leq 7 \times 10^{-6}$ and therefore complements perfectly the present results.

7 Conclusions

A search for the decay $Z^0 \to H\gamma$ has been carried out on the data collected by the DELPHI experience in the years 1991 to 1994. The results are compatible with the expected background allowing to set a limit on the branching ratio for this process in the range of $0.5 - 3 \times 10^{-5}$ for H masses between 5 and 70 GeV. This limit imposes severe constrains on the *a priori* allowed anomalous $H\gamma$ production and its sensitivity is becoming close to the one needed to test the Standard model prediction.

Acknowledgments

We are greatly indebted to our technical collaborators and to the funding agencies for their support in building and operating the DELPHI detector, and to the members of the CERN-SL Division for the excellent performance of the LEP collider.

References

[1] P. Abreu et al. (DELPHI Collaboration) Zeit. Phys. C53 (1992) 555.
J.L. Contreras, A. De Min, DELPHI note, 94-119 (1994).

[2] M.Z. Akrawy et al (OPAL Collaboration) Phys. Lett. 246B (1990) 285
D. Decamp et al. (ALEPH Collaboration) Phys. Lett. 264B (1991) 476
O. Adriani et al (L3 Collaboration) Phys. Lett. 292B (1992) 472
OPAL PN-140 July 14 1994.

[3] P.J. Franzini et al., Z Physics at LEP 1, CERN 89-08 (1989).

[4] P. Aarnio et al. (DELPHI Collaboration) Nucl. Instr and Meth. A303 (1991) 233

[5] G. Gamberini et al. Nucl. Phys. B292(1987) 237

[6] JADE Collab., W. Bartel et al., Z. Phys. C 33 (1986) 23. Phys. Lett. B318 (1993) 155-162

[7] K. Hagiwara et al. Phys. Lett. B318 (1993) 155-162

[8] P. Abreu et al. (DELPHI Collaboration) CERN–PPE/94–131, To be published in Zeit. Phys. c.

[9] N. Bingefors et al. Nucl. Instrum. Methods A 328 (1993) 447

[10] P. Abreu et al. (DELPHI Collaboration) Phys. Lett. B327 (1993) 386
F. Barao et al. An updated analysis of the $e^+e^- \to \gamma\ \gamma\ (\gamma\ )$ reaction at LEP energies. DELPHI note 95-71 (1995), unpublished.
Contribution presented to this conference.

[11] T.Sjöstrand, Comput. Phys. Comm. 39 (1986) 347;
T.Sjöstrand and M.Bengtsson, Comput. Phys. Comm. 43 (1987) 367.

[12] M.Feindt, O.Podobrin, PXPHOT user's guide, DELPHI note in preparation, unpublished.

[13] A. De Min et al. , DELPHI note, 95-90 PHYS 525 (1995), unpublished.
Contribution presented to this conference.

[14] S.Jadach, B.F.L.Ward and Z.Was, Comput. Phys. Comm. 66 (1991) 276.

[15] F.A.Berends, W.Hollik and R.Kleiss, Nucl. Phys. B 304 (1988) 712.

[16] J.E.Campagne and R.Zitoun, Zeit. Phys. C 43 (1989) 469.

[17] DELPHI Collaboration, DELPHI event generator and detector simulation - User guide, DELPHI note 89-76 (1989), unpublished.

[18] M. Aguilar-Benitez et al., Phys. Rev. D45 (1992) III.39

[19] B.A. Kniehl, Phys. Rep. 240 (1994) 211;
E. Gross, B.A. Kniehl, G.Wolf, Zeit. Phys C 63 (1994) 417

[20] DELPHI Collaboration, The DELPHI silicon strip microvertex detector with double sided readout. DELPHI note 95-82 (1995), unpublished.
Contribution presented to this conference.

Figure captions

Figure 1 $q\overline{q}\gamma$ analysis. Mass distribution of the candidates for data (crosses) and simulated hadronic decays of the Z^0 (solid line) after all the cuts except b-tagging have been applied . Also shown, in hatched style, the proportion of fake photons (mainly neutral pions) in the sample.

Figure 2 $q\overline{q}\gamma$ analysis after b-tagging. Mass distribution of the candidates for data (crosses) and simulated hadronic decays of the Z^0 (solid line). Also shown, as a solid line, the smooth aproximation used to compute the limit between 11 and 70 GeV.

Figure 3 $\tau^+\tau^-\gamma$ analysis. Mass distribution of the candidates for data (dots) and simulated events (solid line).

Figure 4 Limits on BR ($Z^0 \to H\gamma$) $\times$ BR ($H \to f\overline{f}$) for the $\tau^+\tau^-\gamma$, $q\overline{q}\gamma$ and $\tau^+\tau^-\gamma$ analysis.

Figure 5 Final SM combined limit. The labels I, II and III refer to the regions described in the text. Also shown, the Standard Model prediction and the region allowed by low energy limits on anomalous Higss couplings

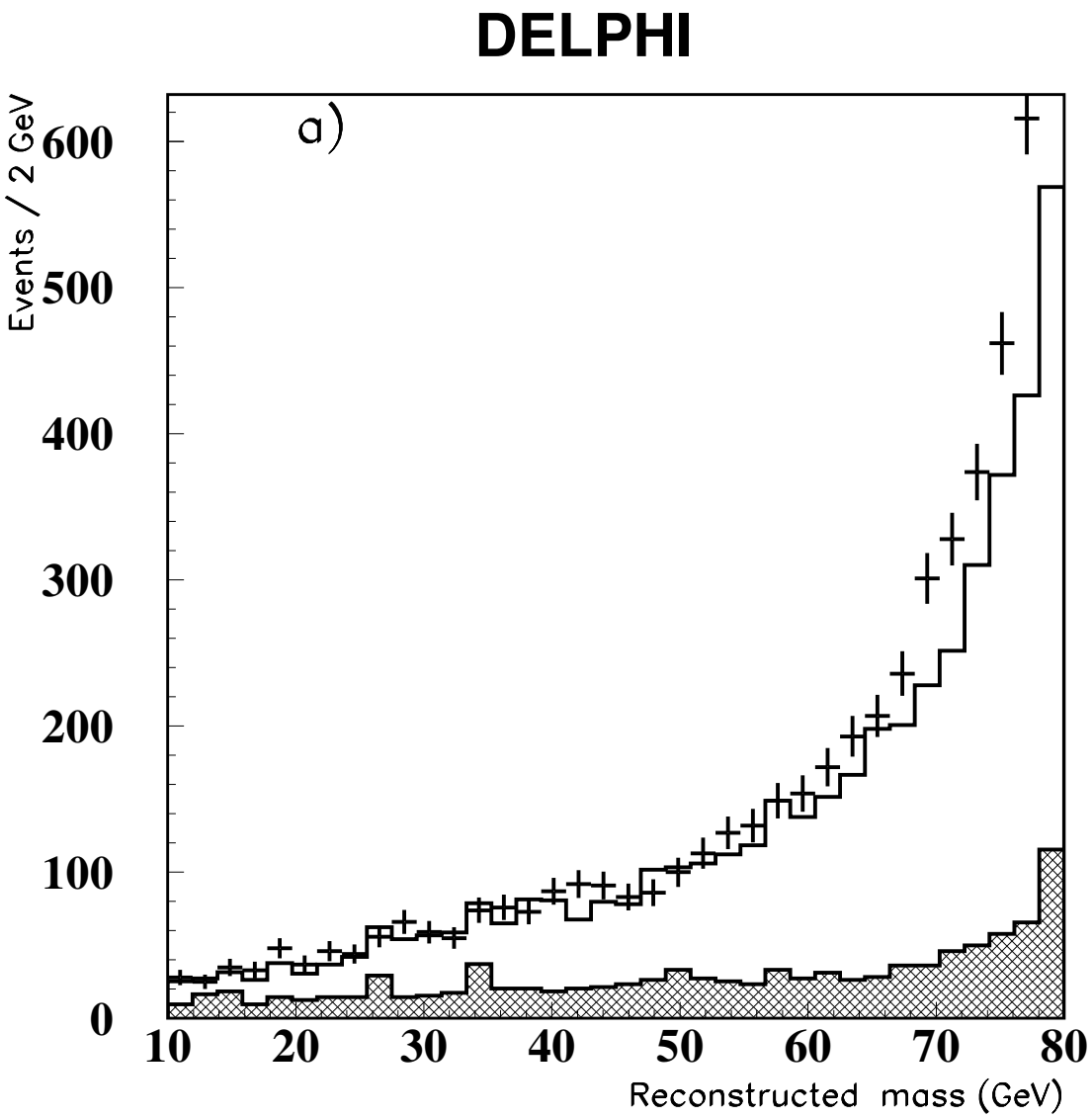
DELPHI
a)
Events / 2 GeV
600
500
400
300
200
100
0
10
20
30
40
50
60
70
80
Reconstructed mass (GeV)

Figure 1:

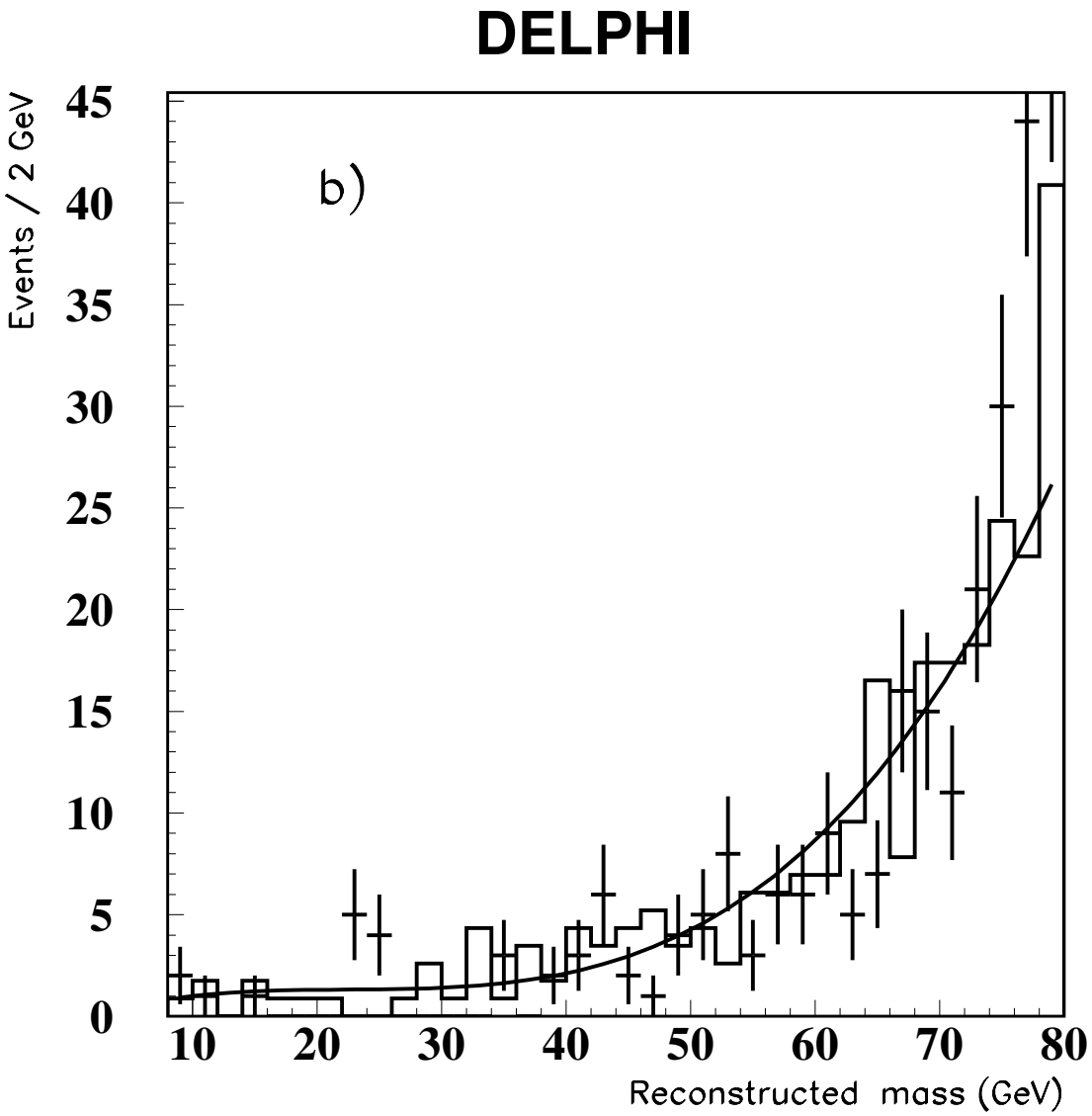
DELPHI
b)
Events / 2 GeV
45
40
35
30
25
20
15
10
5
0
10
20
30
40
50
60
70
80
Reconstructed mass (GeV)

Figure 2:

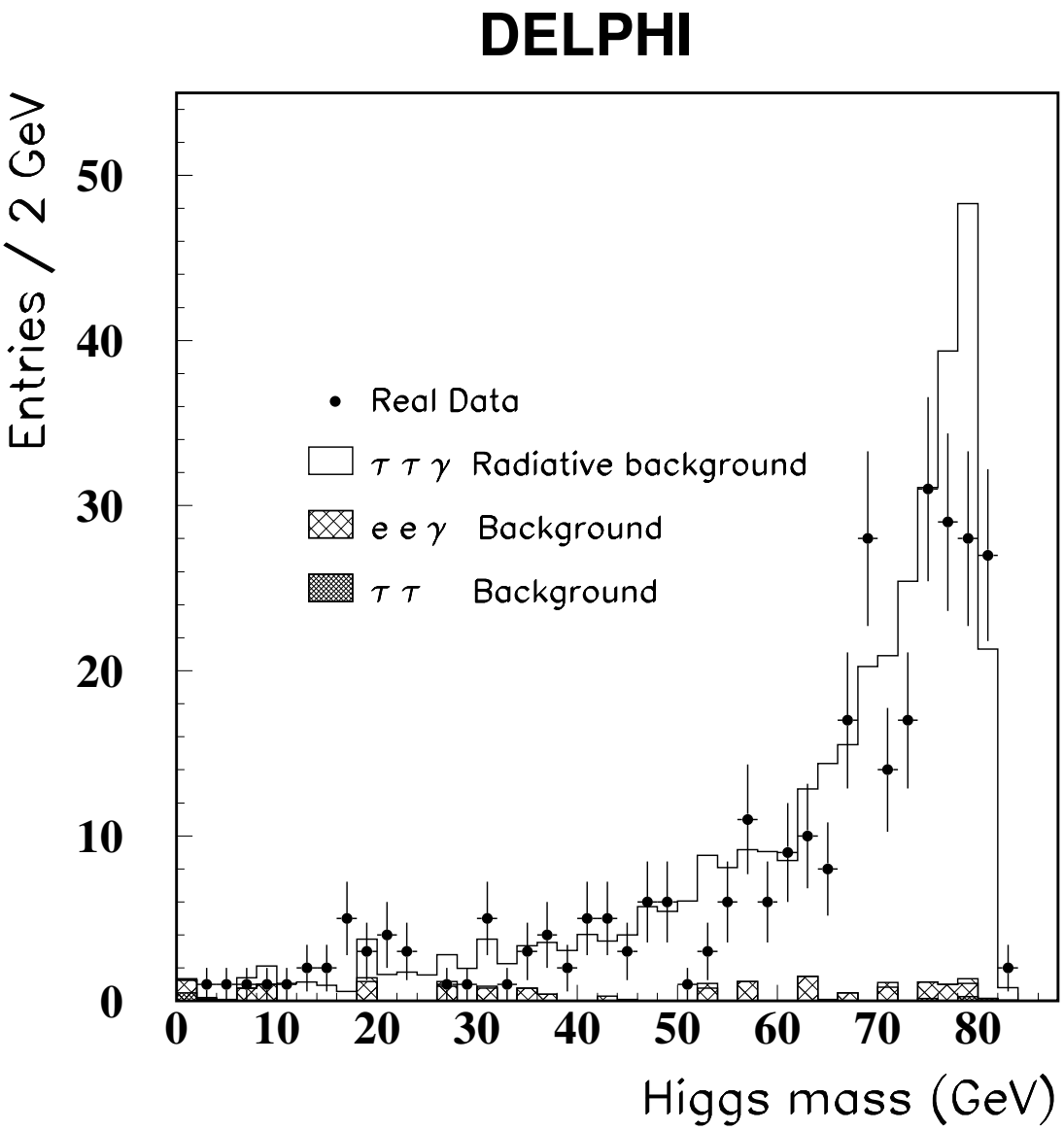
DELPHI
Entries / 2 GeV
50
40
30
20
10
0
0
10
20
30
40
50
60
70
80
Higgs mass (GeV)
Real Data
τ τ γ Radiative background
e e γ Background
τ τ Background

Figure 3:

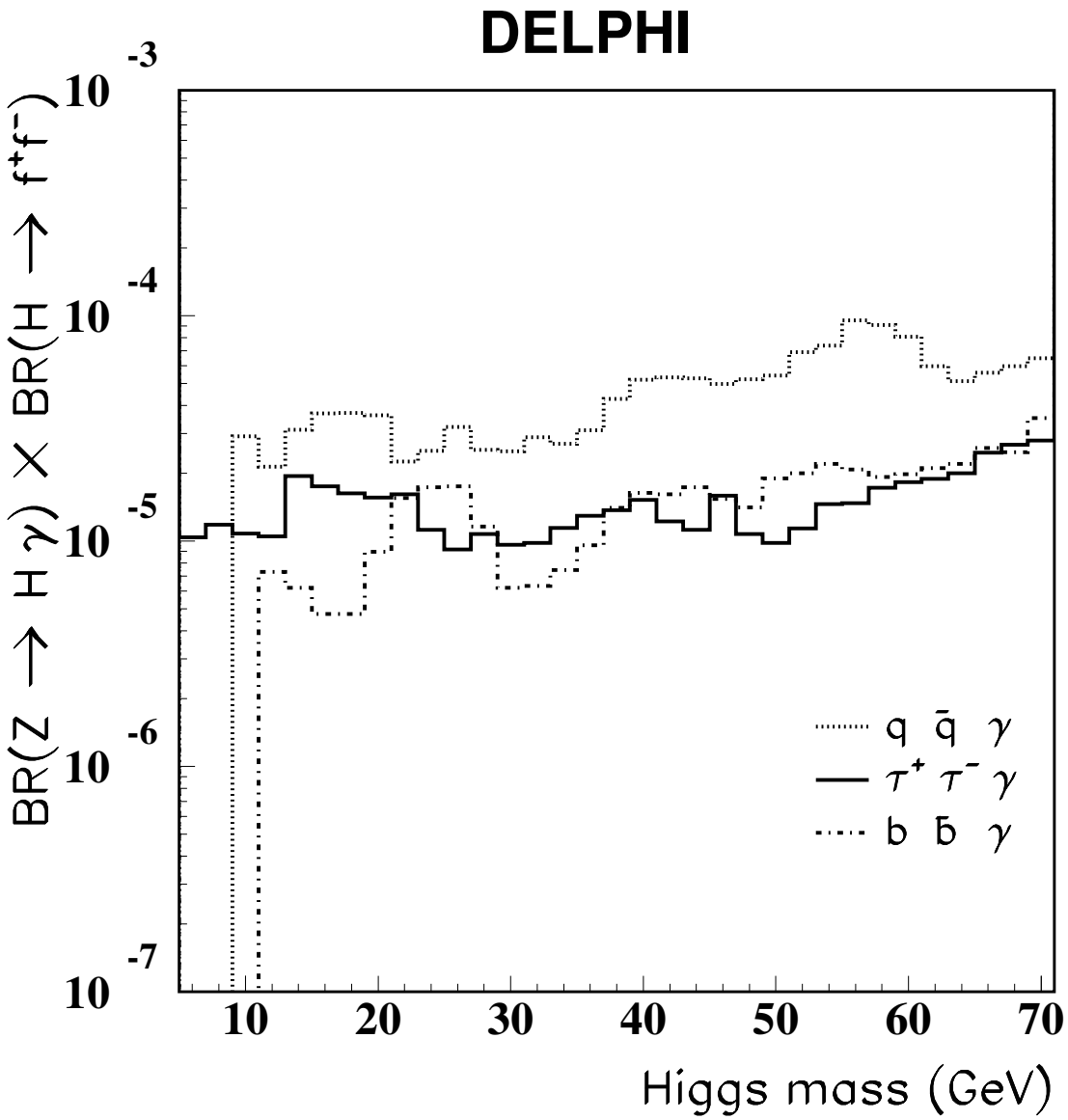
DELPHI
BR(Z → H γ) × BR(H → f⁺f⁻)
10⁻³
10⁻⁴
10⁻⁵
10⁻⁶
10⁻⁷
10
20
30
40
50
60
70
Higgs mass (GeV)
q q̄ γ
τ⁺ τ⁻ γ
b b̄ γ

Figure 4:

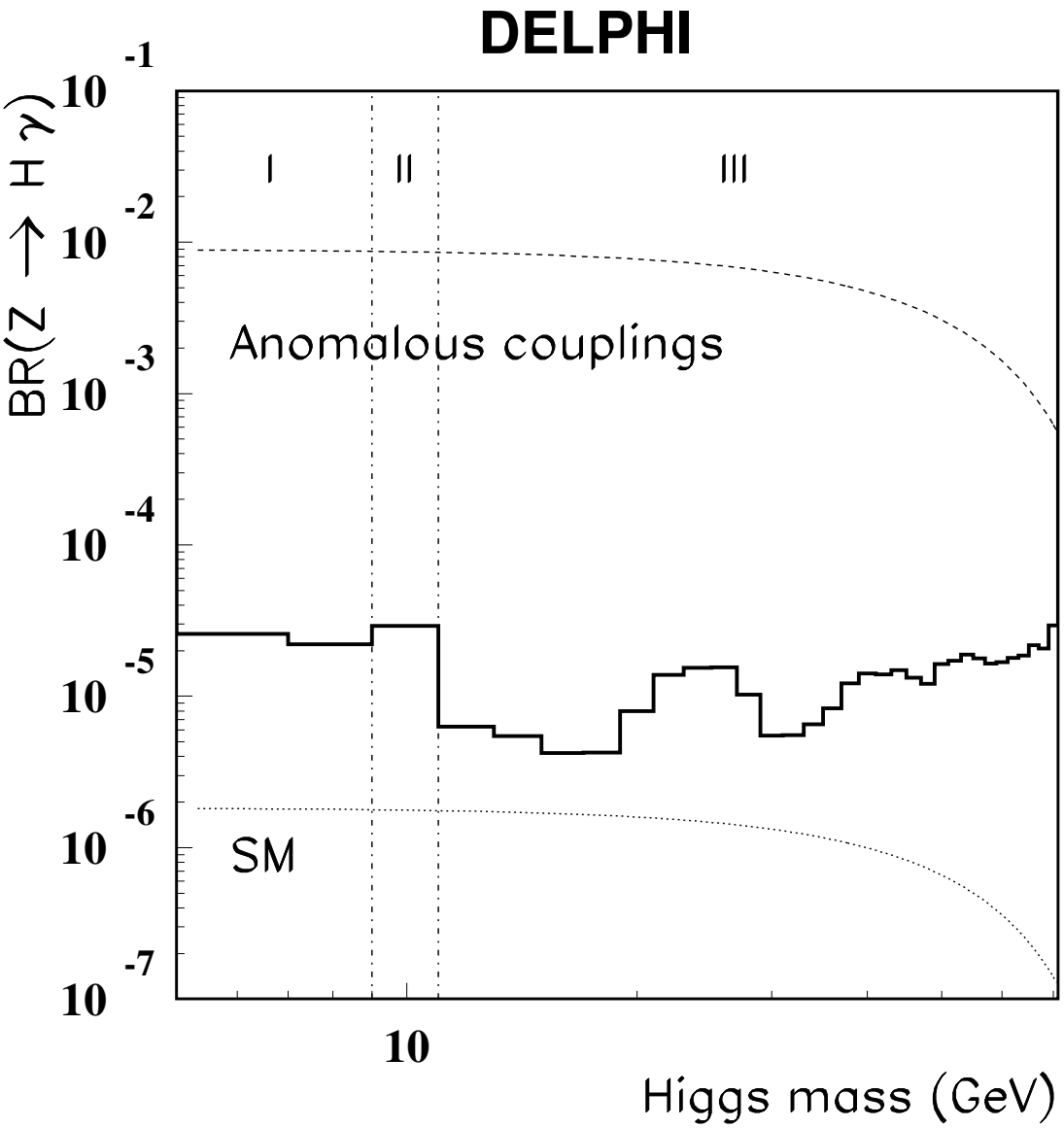
DELPHI
BR(Z → H γ)
10^-1
10^-2
10^-3
10^-4
10^-5
10^-6
10^-7
I
II
III
Anomalous couplings
SM
10
Higgs mass (GeV)

Figure 5: